

Article

# HIPIMS/UBM PVD Coating Equipment Designed to Coat Universal Sized Broaches

Wolf-Dieter Münz<sup>1,2,\*</sup>, Roman Klink<sup>1</sup>, Dejan Aleksic<sup>1</sup> and Mansour Mazaheri<sup>1</sup>

<sup>1</sup> Arthur Klink GmbH, Steinenlandstrasse 1, 75181 Pforzheim, Germany; roman.klink@werkstofflabor.com (R.K.); dejan.aleksic@arthur-klink.de (D.A.); mansour.mazaheri@werkstofflabor.com (M.M.)

<sup>2</sup> Privat Consulting, Birkfelderstrasse 76, 8160 Weiz, Austria

\* Correspondence: w\_dm@gmx.at

**Abstract:** This paper describes a physical vapor deposition (PVD) coating equipment, as well as the according deposition parameters suitable to provide hard nitride coatings on broaches up to a length of 2.2 m. The octagonal-shaped vacuum chamber reached a height of 4.5 m and a diameter of 1.2 m. To explore a sufficient and reproducible film, an adhesion test sample and tools were subjected to a pretreatment in a Cr<sup>2+</sup> Ar<sup>+</sup> high-power impulse magnetron sputtering (HIPIMS) plasma prior to the actual film deposition. Two deposition methods were applied: reactive unbalanced magnetron (UBM) sputtering was introduced to deposit TiAlN-based coatings from Ti50Al50 2.5 m long targets. Alternatively, multilayer coatings were generated by reactive simultaneous UBM sputtering from Ti50Al50 and TiAl6V4 targets, respectively, and chromium targets utilizing high-power impulse magnetron sputtering (HIPIMS) technology. In the latter case, three cathodes were furnished with 0.9 m long targets lined up upon each other. A segmented UBM cathode design was described to meet economic deposition if varying tool sample lots in the deferring workpiece lengths have to be handled in industrial practice. The resulting (TiAl/Cr)N multilayer coatings attained typical hardness values of HV 2800 and an adhesion measured by critical load up to 50 N. The cutting performance of this coating was evaluated by simulated shaping tests over a test length of 210 m on C 45 steel. The (TiAlV/Cr)N showed an improved wear behavior by factor of 2 to 3 compared to TiN deposited by cathodic arc operated in an industrial PVD coater. A real comparison was undertaken, applied to a 1.3 m long model broach. (TiAl/Cr)N showed a prolongation in industrial lifetime by 150% compared to TiN.

**Keywords:** unbalanced magnetron (UBM); HIPIMS; substrate pretreatment; ion implantation; simultaneous UBM/HIPIMS; (TiAlV/Cr)N



**Citation:** Münz, W.-D.; Klink, R.; Aleksic, D.; Mazaheri, M. HIPIMS/UBM PVD Coating Equipment Designed to Coat Universal Sized Broaches. *Coatings* **2022**, *12*, 300. <https://doi.org/10.3390/coatings12030300>

Academic Editor: Susana Sério

Received: 22 November 2021

Accepted: 3 February 2022

Published: 23 February 2022

**Publisher's Note:** MDPI stays neutral with regard to jurisdictional claims in published maps and institutional affiliations.



**Copyright:** © 2022 by the authors. Licensee MDPI, Basel, Switzerland. This article is an open access article distributed under the terms and conditions of the Creative Commons Attribution (CC BY) license (<https://creativecommons.org/licenses/by/4.0/>).

## 1. Introduction

Broaches are elongated, slightly tapered cutting tools used for removing materials and precision finishing of the inner surface of circular or noncircular holes in engineering parts for automotive and other industries [1]. The dimensions of these tools may vary in an astonishing wide range, covering diameter dimensions up to 0.5 m and up to 2.5 m in length. Broaches are fabricated single piecewise either of high-speed steel (HSS) or tungsten carbide (WC). To prolong the lifetime of these expensive tools in industrial use, it is state of the art to protect them with hard coatings. Physical vapor deposition (PVD) is a useful deposition technology. Today, the cathodic arc process is the favoured method of deposition, introducing TiN as coating material. Figure 1 illustrates such an example, showing also the huge geometrical dimensions inside the coating equipment described below, outlining differing tool dimensions (Figure 2a). The open vacuum chamber with an inner diameter of 1.2 m is loaded; e.g., with a TiN-coated broach 0.5 m in diameter. Besides TiN, the multicomponent coating CrAlN has found broad industrial application as well.

Due to its high Al content (approx. 70 at.%), this coating is particularly suited to application if dry cutting at enhanced cutting speeds is demanded [2] (Oerlikon Balzers GmbH).



Figure 1. Outlining huge equipment dimensions and potential tool sizes.

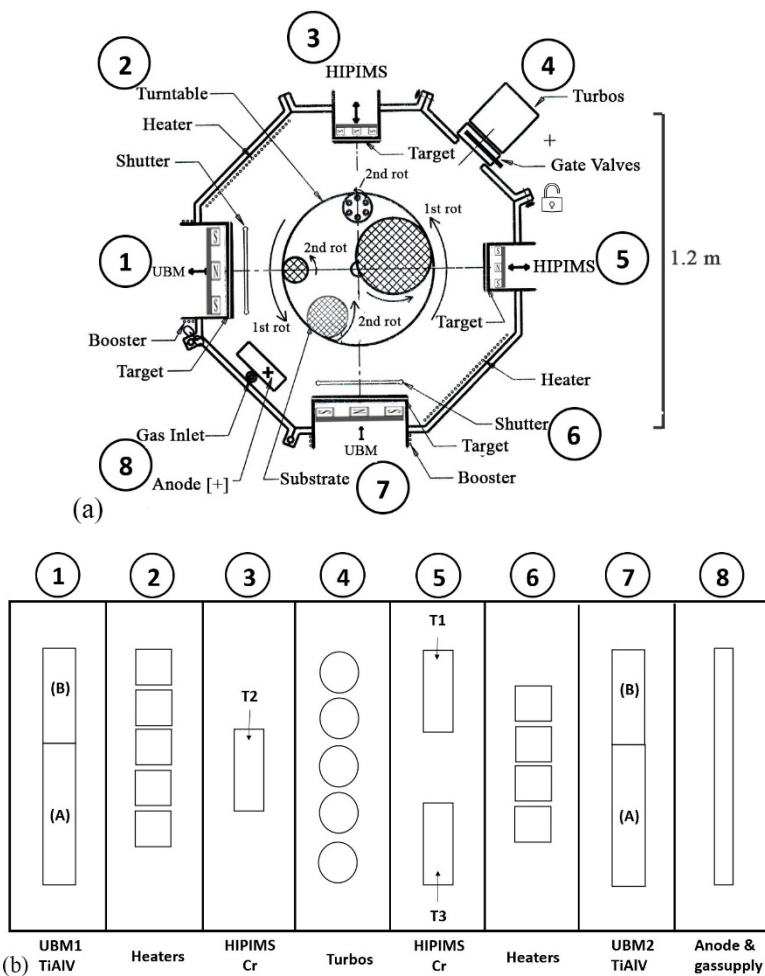


Figure 2. (a) Schematic horizontal cross section showing cathodes, pumps, shutters, and turntable. (b) Vertical view outlining component distribution and target segmentation.

The coating technology described in this paper was based on early experiments on TiAlN [3,4]. TiAlN-coated twist drills coated by UBM clearly outperformed TiN-coated

tools under dry-cutting operations (number of achieved holes: uncoated 25; TiN 143; TiAlN 365). This must be correlated with an increased resistance against oxidation, as has been confirmed according to gravimetric studies. TiAlN coatings show temperature stability up to 700 °C, whereas TiN begins to oxidize already at 500 °C, similar as HSS. Additionally, V has been incorporated into the here-investigated TiAl-based coating. V enhances the hardness of the coating [3]. Furthermore, it promises to reduce the friction coefficient of a TiAlN/VN coating, where the friction coefficient drops from 0.9 at 500 °C to 0.18 at 700 °C [5]. Therefore, the actual temperature on the cutting edge itself should be reduced as well. This is certainly a beneficial side effect. A broad survey on TiAlN-based coatings was published in [6].

Besides titanium, aluminum, and vanadium, chromium played a substantial role in this PVD project. Introducing HIPIMS chromium dominated not only the film architecture, but it also controlled the reproducibility of the film adhesion. Altogether, coatings consisting of these elements allow a droplet-free film deposition of hard coatings, if using a UBM and HIPIMS technology suited for dry, fast, high-temperature cutting operations is demanded.

Prior to the development program based on (TiAlV/Cr)N multilayer coatings specialized to coat expensive broaches, methods of the cathodic arc technology have been considered with respect to its well-known positive adhesion properties. There, a pretreatment of the substrate surface takes place under the influence of multiple ionized metal atoms. In this context, comprehensive results on metal ion concentrations in arc discharges have been published in [7], reporting, e.g., multi-ionization on  $\text{Cr}^{2+}$ ,  $\text{Ti}^{3+}$ , and  $\text{W}^{6+}$ . Utilizing such ions by applying a negative substrate/tool bias in the range of typically  $\geq 1000$  V, metal atoms are implanted into steel substrates in advance of the actual film deposition. If one deposits on such a pretreated steel surface, transition-metal nitride-coating-enhanced adhesion was observed, promoted by metal ion bombardment and correlated epitaxial growth [8]. An industrial research program was carried out with respect to equipment design [9–12]. This combined deposition method was introduced to the PVD coating industry and designated as arc bond sputtering (ABS) technology [10]. However, this approach suffers under a generation of “droplets” inherent to the cathodic arc process. However, the resulting droplet concentration was markedly reduced in comparison with an overall cathodic arc deposition procedure, if applied as pretreatment only [13]. To eliminate the droplet effect completely, the HIPIMS [14–17] process was introduced into the deposition technology in the present project. Similar to cathodic arc plasma, the HIPIMS process provides metal ions. Choosing chromium as target material,  $\text{Cr}^+$  and  $\text{Cr}^{2+}$  were analyzed in [18]. After applying a negative substrate bias, chromium was implanted, therefore similar to the case of the cathodic arc process. In addition, a substrate cleaning took place by the superimposed etching effect caused by the bombarding  $\text{Ar}^+$  ions present in the UBM glow discharge. Therefore, a substantial but also reproducible increase in adhesion of the deposited UBM hard coating was observed [18,19]. In addition, particular attention has been paid to the simultaneous operation of HIPIMS [20–22] and UBM sputter deposition. State-of-the-art target materials were used in this special project. As described below in more detail, one UBM cathode was furnished with a powder-metallurgically prepared Ti50Al50 target. A TiAl6V4 metal alloy target was attached to a second UBM cathode. Powder-metallurgically prepared chromium targets were attached to three HIPIMS cathodes.

## 2. Materials and Methods

### 2.1. Equipment Design

Figure 2a outlines the horizontal cross section of the octagonal vacuum chamber schematically. The height of the chamber amounted to 4.5 m and the diameter was 1.2 m. Two large doors of full-chamber height were mounted to a slim chamber frame, thus allowing full access to the chamber inside. Two cathode bodies 2.5 m in length and 0.17 m in width were installed from the chamber outside into the chamber doors. One cathode per door provided UBM operation. The two cathodes were furnished with 12 mm thick Ti50Al50 and with TiAl6V4 targets. These targets were segmented into two parts at a length

ratio of 2 to 1 as explained later, and as indicated by Figure 2b schematically. Three 0.9 m long and 0.12 m wide cathodes were furnished with 8 mm thick chromium targets opposing the UBM targets.

Figure 2b describes that in one case, two HIPIMS cathodes, including targets T1 and T3, were installed at a precisely defined distance in one door. The third cathode, T2, was placed in a parallel direction in the second door. If lined up in one row, the ends of T1 and T3 would slightly overlap the ends of cathode T2, which can be seen in Figure 2b. Two vertically adjustable steel plates protected each UBM cathode as shutters against cross contamination, when the chromium targets had to be sputter-cleaned by Ar<sup>+</sup> prior to the actual deposition process, or when the cathodes were operated sectionwise.

As indicated by Figure 2a, there was free excess to the cathode bodies, showing also on the surface of the mounted target the magnetron-specific racetrack shaped by the permanent magnetic field arrays [3,4]. The magnetic field arrays could be controlled with respect to their distance to the cathode rear simply from the chamber outside (explained briefly in [11]). This opened up the opportunity to introduce a “fine trim” of the distance between the magnetic array to the cathode rear, and therefore also the increasingly developing groove-shaped target on the front side. While the target erosion was progressing during continuing usage, the magnetic field strength would increase in the direct depth of the groove. The magnet arrays were equipped with a “lifting” system [11]. An automatically controlled distance guaranteed a constant magnetic field strength of 35 mT, practically in the bottom of the target groove [11] according to the degree of target erosion. All cathodes, both UBMs and HIPIMS, were equipped with such an automatic magnetic lifting system. In addition, the UBM cathodes were surrounded by electromagnets extending over the total cathode length. These coils were again mounted from outside to the chamber doors. Designated as “booster coils” (12 windings), these electromagnets allowed us to push the magnetic fields and therefore the generated plasma deeper towards the chamber centre. Figure 2a,b also shows an anode positioned directly between the two UBMs. On the rear side of the anode body, the central gas inlet tube was mounted. Figure 2a,b also indicates the position of the turbo molecular pumps. Five pumps were vertically distributed over a 2.5 m target length, which is outlined in Figure 2b. Furthermore, the position of heating elements is shown in Figure 2b. Special care was taken in the design of the turntable. One should take into account that the turntable might have to carry up to one ton of tool weight, depending on the diameter and length of the broaches. The turntable rotated at 2 rpm. At least a twofold rotation of the tools was essential. The substrate rotation amounted to 7 rpm per one rotation of the table. It was also important that the twofold rotating tools remained close to the cathodes when passing them during the first rotation movement. A distance range of 120 to 170 mm was anticipated. This allowed direct and intensive contact with the plasma in front of the targets, which was a precondition for dense film growth. It is worthwhile to recall the enormous distances existing between the targets and the “shadow” side of the rotating tools. Only the appropriately combined operation of cathode discharges, booster coils, and anodes would guarantee successful deposition of dense hard coatings.

Figure 3a shows a view into the open chamber. Figure 3b shows an overall survey of the closed equipment, including the control panel. Besides three TiN-coated broaches, there were also two vertically placed UBMs outlining the “race traces” typical for planar magnetrons. Hidden by the broach on the right-hand side, one of the HIPIMS cathodes becomes visible; however, it was covered by a shutter and was not easy to identify. Power supplies, the roots blower, and rotation pumps were located in the cellar below the equipment.

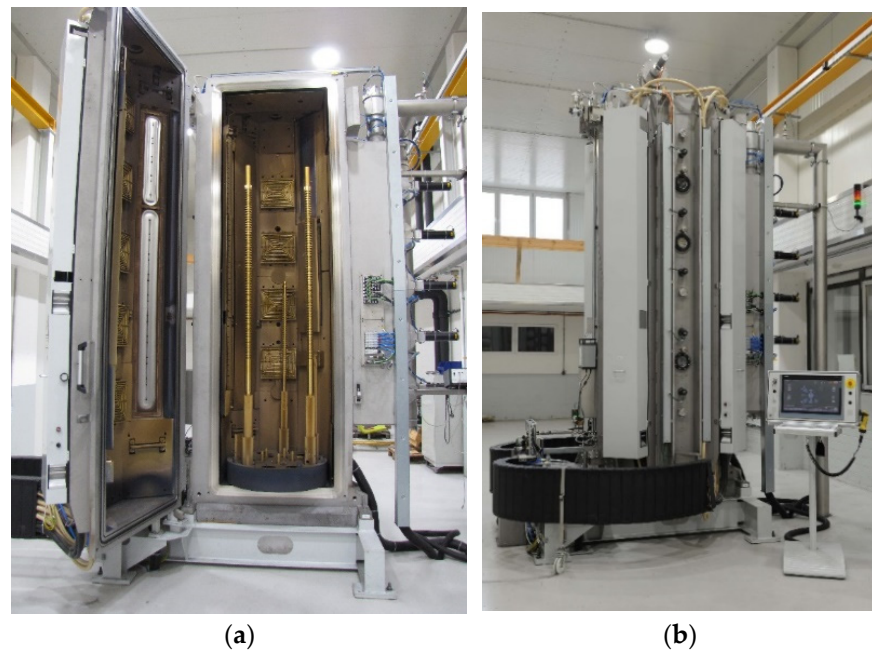


**Figure 3.** (a) Opened and (b) closed equipment setup.

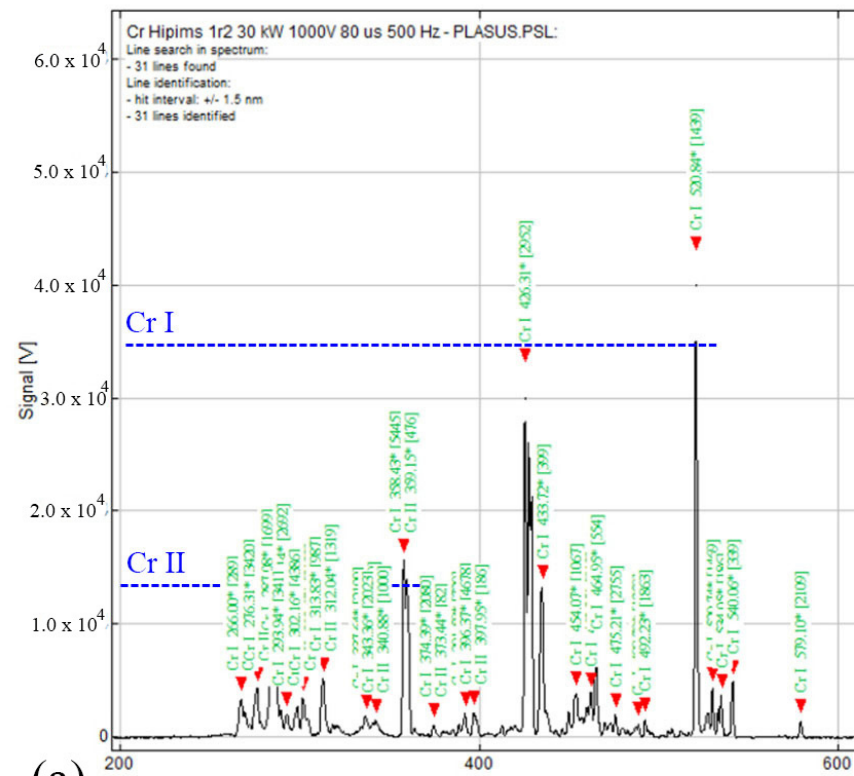
### 2.2. Power Supplies

Both UBMs were equipped with 3 independently controlled, 15 kW DC power supplies per cathode. To generate the UBM plasma, the supplies were operated in constant current mode. The booster coils were fed by 180 A DC. The anode located between the two UBMs was connected to a DC power supply (250 V/200 A max). The HIPIMS cathodes, as well as the turntable carrying the substrates, were each connected to 20 kW pulse generators. They were process oriented, and they could be switched from pulse mode to DC mode. In pulse mode, they were operated at a pulse frequency of 100 to 500 Hz. The pulse width could be set to 50, 80, 160, up to 600  $\mu$ s. The pulse height reached up to  $-1000$  V. The typical pulse current amounted to 950 A.

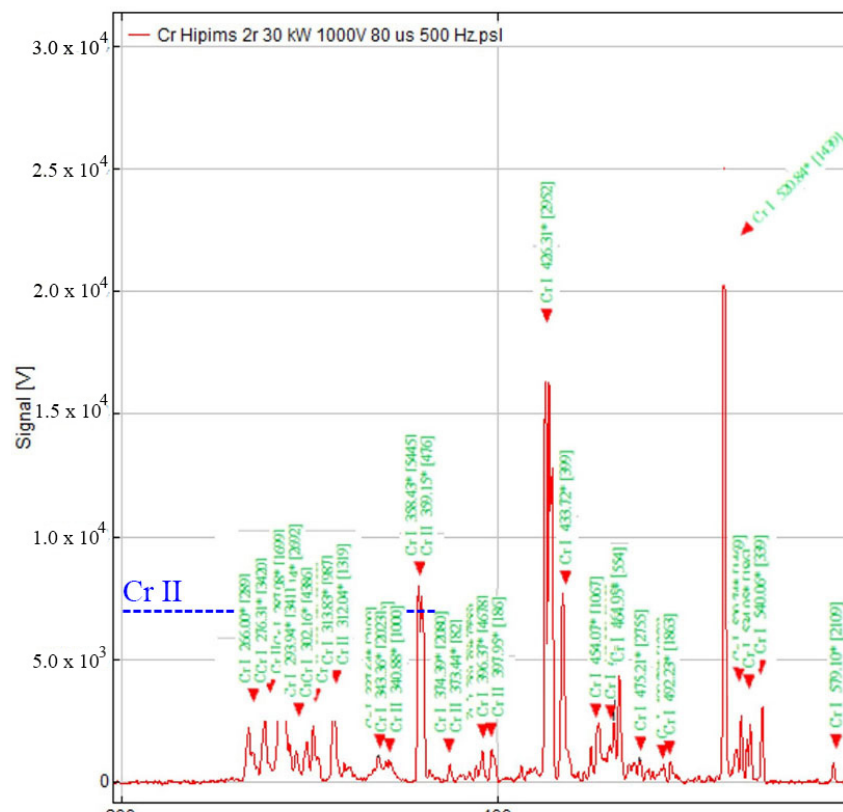
### 2.3. Analyses of HIPIMS Plasma

The application of HIPIMS dominated the practicability of the here-described PVD deposition technique essentially. A better understanding of the deposition conditions was provided by the optical emission spectra (OES) [23]. Particular importance was ascribed to the degree of Cr ionisation itself, as well as to the extension of the plasma into the chamber space.

For test purposes, a model HIPIMS discharge was prepared using the following HIPIMS parameter settings only on cathode T2: pure Ar atmosphere  $2.10^{-3}$  mbar; 15 kW on T2 cathode,  $-1000$  V/500 Hz/80  $\mu$ s. The OES sensor was placed in two positions, at a “near” distance of 300 mm (Figure 4a) and at a “far” distance of 700 mm (Figure 4b) from the T2 cathode. The plasma was described using the indices Cr I  $\equiv$  Cr<sup>0</sup>; Cr II  $\equiv$  Cr<sup>+</sup>; and Cr III  $\equiv$  Cr<sup>2+</sup>. Peaks for Cr I and Cr II were indicated in both positions. Cr III, as predicted by [18], could not be detected in this special test arrangement. This may be explained either by the fact that Cr III ions were caught back by the cathode near magnetic field, or that the Cr III ions interacted in collisions with Ar atoms, which were present in high concentration. Therefore, the Cr III ions in low concentration might have been distributed along the rather long distance between the cathode and OES monitor positions.



(a)



(b)

**Figure 4.** OES spectra of HIPIMS plasma (15 kW per cathode/−1000 V/500 Hz/80 μs detected (a) at a close distance of 300 mm and (b) at a far distance.

However, at least Cr II was not detected in the case of a pure UBM plasma. The Cr II intensity amounted to a maximum of 40% of neutral Cr (Figure 4a) at a distance of 300 mm. Cr II signals were detected at wavelengths of 340, 359, 373, and 397 nm, with 359 nm as the main peak. If we compared the Cr II intensity at a distance of 700 mm, an intensity of 20% (Figure 4b) was observed as compared to the value at a distance of 300 mm. Cr II expanded therefore over half of the turntable diameter, thus allowing the assumption that at least a gentle metal-ion bombardment occurred during most of the substrate rotation period during HIPIMS pretreatment.

#### 2.4. Segmentation of the UBM Process

To enhance the economy of the PVD production process, the UBM cathodes can be operated in two different extended target zones, as already indicated schematically in Figure 2b. In general, the cathodes may be furnished either with uniform single-piece targets or with targets in several pieces, depending on their availability, composition, or costs of manufacturing. In the case presented here, the overall target segmentation obeyed the ratio of 2:1. The longer segment (1.55 m) was assigned to coat tools up to a length of 1.4 m (CASE A). The rest of the target (0.95 m) was reserved to coat shorter tools up to 0.8 m in length, or to coat test samples for research purposes (CASE B). In the case of tools up to a length of 2 m, the coating procedure occurred in multiple sequential 2–5 min steps switching from (CASE A) to (CASE B). Figure 5 outlines the segmentation principles.

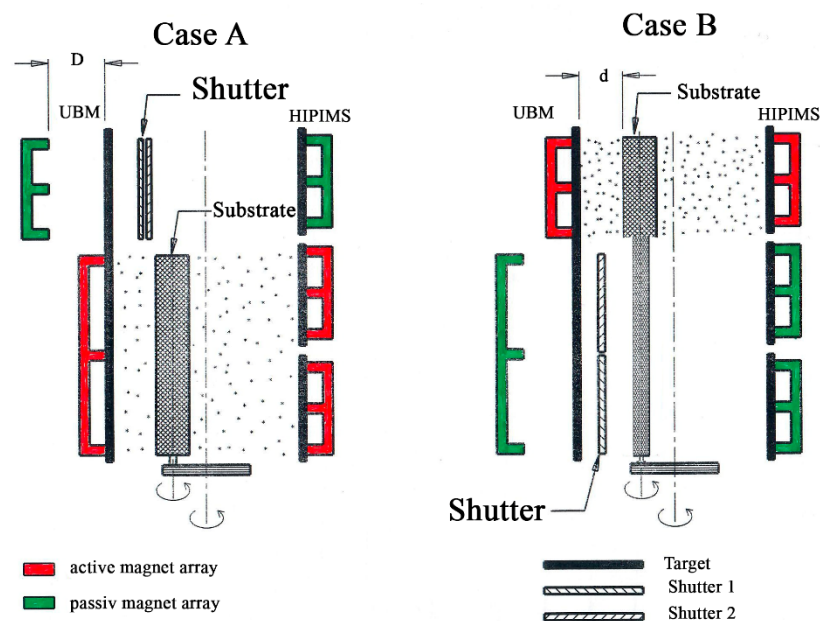


**Figure 5.** Interaction of active/passive target zones controlled by magnet and shutter positioning.

The UBM cathode bodies themselves extended over the complete length of 2.5 m. Two individual magnet array systems were placed inside these UBM cathode bodies. Their extension ranged at a 2:1 ratio. The distance between the magnet arrays was precisely optimized in order to provide uniform deposition rates over the entire cathode length. The magnetic fields generated by the long booster coils did not disturb this optimization procedure. As mentioned above, all magnet arrays installed in the equipment were furnished with magnetic lifting units. Besides the so-called “fine trim” controlling the target erosion progress, a so-called “coarse trim” allowed the activating and deactivating of the UBM discharge in the desired target area. Deactivation of the UBM effect was achieved by a cathode behind the magnet array at a distance of 100 mm. In comparison to the UBM activation procedure, the relevant HIPIMS adjustment turned out to be simple.

In (CASE A), two HIPIMS cathodes, T1 and T2, opposing the longer segments of the activated UBM cathodes were switched on. In (CASE B), only one HIPIMS cathode, T3, was in operation, opposing the shorter segments of the activated UBMs. Figure 5 illustrates the segmentation technique in colour. Red denotes the active situation, whereas GREEN denotes the passive case. The installed shutters provided protection for the passive UBM sections against cross-contamination during the deposition process caused by the active target segments. Coating of 2 m long broaches was achieved by the sequential operation of (CASE A) and (CASE B), as outlined above. The complete process was fitted out by automatic control in activating the involved power supplies, the “fine” and “coarse” trim of the magnet arrays, and the up-and-down movement of the shutter plates.

The segmentation of the deposition process offered a further advantage. The majority of actual tool-coating production lots will take place in (CASE A) mode. Moreover (CASE B) can be utilized to explore the performance of interesting research using shorter and therefore cheaper targets, as well as shorter test broaches. Eventually in (CASE B) mode, the incorporation of special materials into the coating, such as oxidation-reducing yttrium [24,25] or silicon, may be explored, particularly with respect to dry high-speed performance of broaches. Alternatively, the influence of plasma nitriding [26] prior to the tool-coating process might be of interest.

### 2.5. (CASE A) Deposition

Three types of hard coatings were investigated. Type 1 consisted of TiAlVN, while Types 2 and 3 consisted of (TiAlV/Cr)N. Before in vacuo treatment, a wet chemical cleaning of the selected substrates took place. The in vacuo treatment distinguished between four steps: (1) heating up the substrates to 400 °C in Ar<sup>+</sup> 20% H<sub>2</sub>; (2) the actual HIPIMS pretreatment; (3) the formation of a so-called “ramping socket”; and (4) the actual deposition of the actual nitride hard coating. It is important to note that the test substrates were fixed to a cylindrical tube 60 mm in diameter to simulate film growth conditions comparable to those on the surface of the test broach with an identical diameter. The turntable rotated at 2 rotations per minute (first rotation). Substrates and the broach were subjected to a second rotation as outlined above. Steps (1), (2), and (3) were identical for all three types of coatings.

#### 2.5.1. In Vacuo Pretreatment

When starting the deposition process, the chamber was pumped down to a residual pressure of  $5 \times 10^{-6}$  mbar. A typical leak rate of  $5 \times 10^{-5}$  mbar.l/s was evaluated. All parts were subjected to a heat treatment. The heaters indicated in Figure 2b operated at 570 °C, achieving a substrate temperature of 400 °C after a heating duration of 1.5 h.

A glow discharge in a pure Ar atmosphere ( $2 \times 10^{-2}$  mbar;  $-800$  V, 30 min) provided further preconditioning of the substrate surfaces. Based on the experience gained in [8,18], the samples were subjected to a 25 min HIPIMS bombardment initiated in an Ar atmosphere ( $2.5 \times 10^{-3}$  mbar, Ar flow: 400 sccm). Each of the two corresponding HIPIMS cathodes initiated (compare with Figure 5) operated at 12 kW,  $-1000$  V, pulse 500 Hz/pulse 160  $\mu$ s. The anode was set to +200 V. The pulse height of  $-1000$  V was kept constant over the total activation by applying the “fine trim”. The substrates were biased pulsewise ( $-800$  V; 600  $\mu$ s). During this procedure, chromium implantation and Ar etching took place.

#### 2.5.2. Formation of the Ramping Socket

This phase of film deposition lasted over 15 min in total. The activation of the two chromium HIPIMS cathodes was continued with identical parameter settings. Both UBM discharges were initiated by ramping up the discharge current linearly from 10 to 30 A until a discharge voltage of  $-550$  V was reached by using 2 of the 15 kW power supplies. The booster coils were fed by 180 A DC. At the same time, the nitrogen flow was ramped up linearly from 160 to 360 sccm. The voltage level was controlled by “fine trim” at a constant level of  $-550$  V. Under such conditions, a UBM current density of 6 mA/cm<sup>2</sup> was provided

over the complete target life. In parallel, the bias voltage provided by the dedicated HIPIMS power supply was switched into DC mode after 7 min of socket formation, and was ramped down from  $-500$  V DC to  $-125$  V DC linearly.

#### 2.5.3. Deposition of Type 1 Coating

HIPIMS remained deactivated. UBM gas flow and bias settings continued to be unchanged. However, it was advantageous to use the two deactivated HIPIMS cathodes as anodes at a level of  $+200$  V to pull the UBM plasma deeper into the chamber centre. The deposition time was 1 h 44 min, achieving a film thickness of  $2.2$   $\mu\text{m}$ . The resulting deposition rate amounted to  $0.35$  nm/s. The color of the coating turned out to be dark violet.

#### 2.5.4. Deposition of Type 2 Coating

The deposition of the Type 2 film was carried out by simultaneous operation of both UBM cathodes and the corresponding two HIPIMS cathodes, T1 and T2 [20–22]. The parameter settings were identical to those during the end phase of the socket formation. The deposition time was 52 min, the thickness of the film grown reached  $1.6$   $\mu\text{m}$ , and the resulting deposition rate amounted to  $0.51$  nm/s. The coated test samples showed a silvery tone.

#### 2.5.5. Deposition of Type 3 Coating

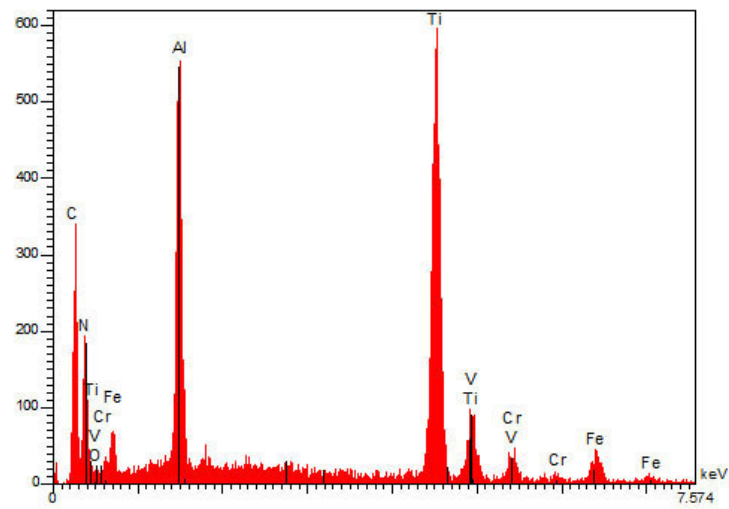
This type of coating was deposited by again utilizing the simultaneous operation of UBM and HIPIMS cathodes. During plasma pretreatment (2), the HIPIMS cathodes were still operated at  $12$  kW per cathode as in the Types 1 and 2 cases. However, during socket formation (2) and the actual film deposition, the HIPIMS power was reduced to  $6.5$  kW (pulse:  $-1000$  V,  $250$  Hz,  $160$   $\mu\text{s}$ ). The UBM parameters remained unchanged. Due to the reduced HIPIMS power, the nitrogen flow was ramped up to  $280$  sccm only. Another change was to reduce the substrate bias from  $-500$  V DC to  $-75$  V. Finally, after depositing the major part of the coating (deposition time:  $75$  min), a thin topcoat was deposited using UBMs only. The DC parameters remained unchanged. This additional coating process was carried out over  $5$  min. The evaluated total film thickness amounted to  $1.6$   $\mu\text{m}$ , and the resulting deposition rate turned out to be  $0.23$  nm/s. The color was dark violet, similar to the case of the Type 1 film.

### 3. Results and Discussion

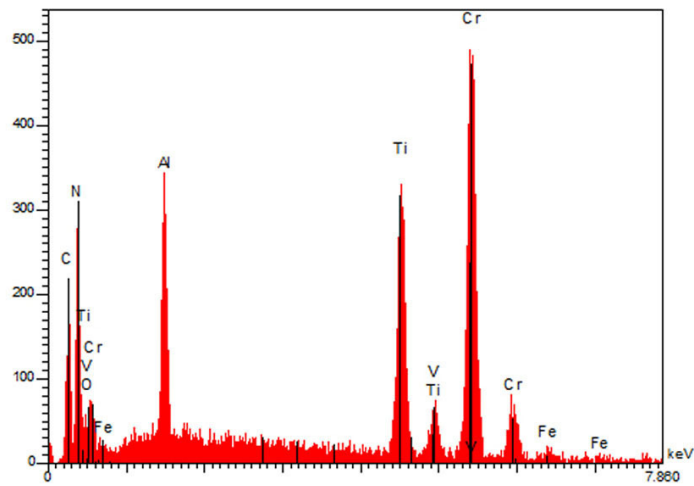
#### 3.1. Composition and Microstructure

The chemical composition of the test samples was evaluated by EDX analyses (Jeol YSM 800 with EDS-Analysator, Karlsruhe, Germany), and is summarized in Figure 6. The results concerning the Type 1 (Figure 6a) and Type 2 (Figure 6b) coatings confirmed the expectations drawn from their process parameters.

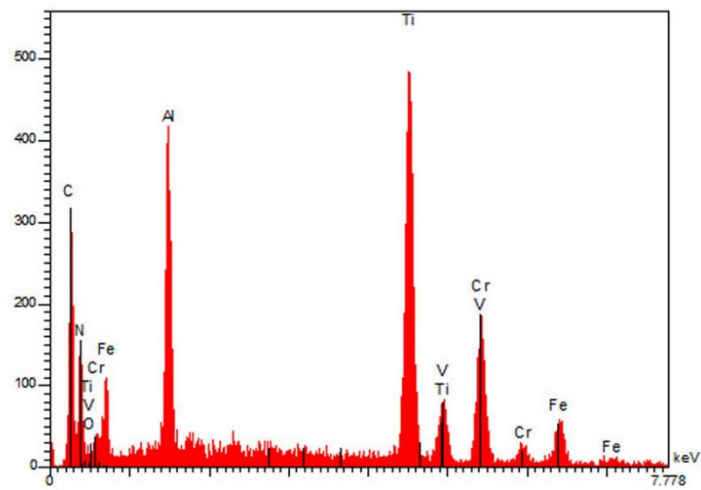
Figure 6a clearly highlights the dominance of titanium and aluminum. Vanadium presented a weak signal, caused by its low concentration in only one of the Ti-rich UBM targets. On the other hand, Figure 6b clearly shows a strong contribution of chromium caused by the HIPIMS interaction. Figure 6c shows the **Type 3** coating, which surprised us with a rather low concentration of chromium, although the HIPIMS power was reduced by a factor of two only. The chromium r signal was lower than the signals contributed by titanium and aluminum.



(a)



(b)



(c)

**Figure 6.** Composition of investigated film types: (a) Type 1: Chromium-free; (b) Type 2: high chromium content; (c) Type 3: low chromium content.

Figure 7 reveals cross sections and the surface structure obtained by scanning electron microscopy (SEM) analyses (Zeiss DSM, Jena, Germany). Figure 7a shows a **Type 1** TiAlVN coating as grown in the well-known tensile but dense and compact columnar microstructure, familiar from pure TiAlN-like coatings [3,8].

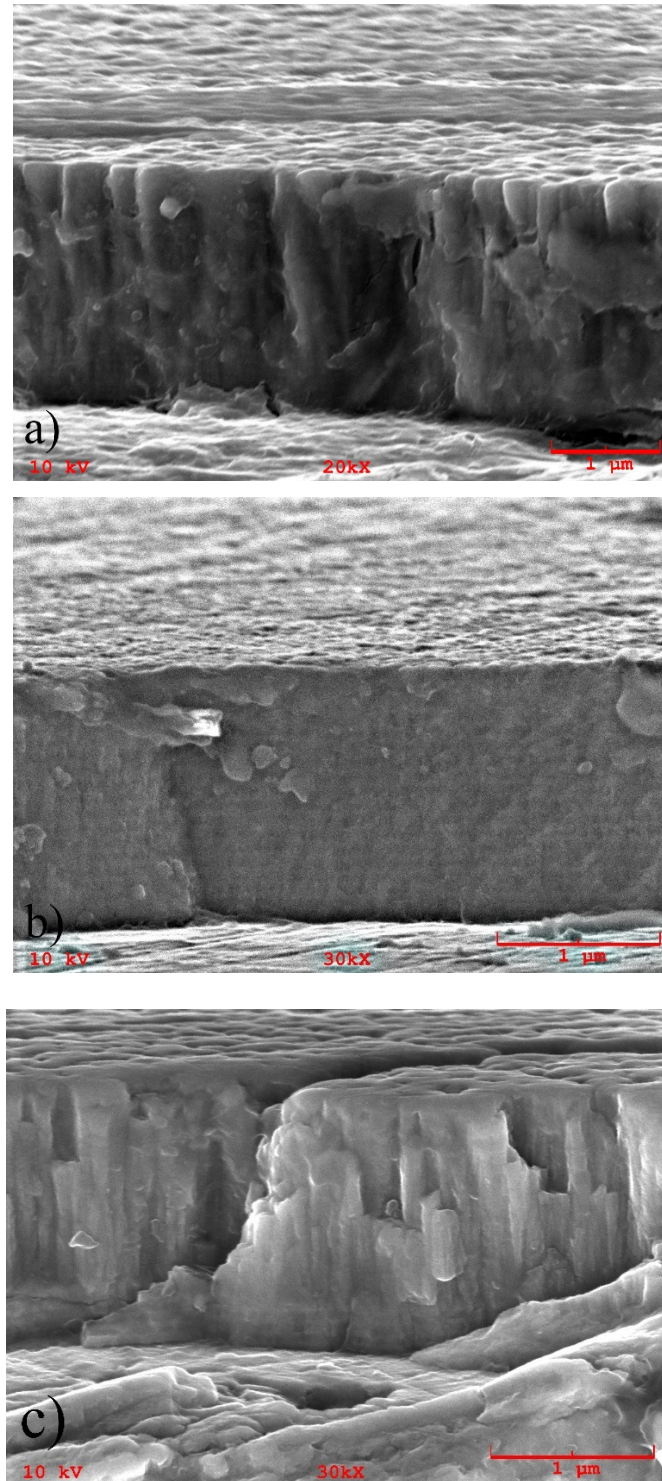


**Figure 7.** Film cross sections examined by SEM: (a) **Type 1:** TiAlVN; (b) **Type 2:** (TiAlV/Cr)N, high chromium content and multilayer; (c) **Type 3:** low chromium content, and few multilayers.

The surface morphology was consistent with the tensile film growth. The apparently dense structure may be attributed to the positive influence of the anode supplying sufficient plasma density despite the large varying distances between the substrates and cathodes occurring as a consequence of the slowly rotating turntable (first rotation). In contrast, Figure 7b reveals a layered structure of **Type 2** coating. The columnar microstructure is missing completely. The surface morphology let us assume a fine grain structure. Due to the layered structure, the **Type 2** film was designated as (TiAlV/Cr)N, in contrast to **Type 1** as TiAlVN. Figure 7c describes the morphology of the **Type 3** coating as quite different from that of **Type 1** and **Type 2**. The film again exhibited a columnar growth, similar to **Type 1**. However, the film structure was substantially coarser. In addition, the film seemed to be more brittle than in the **Type 1** sample. Furthermore, the tensile structure seemed to be not very dense, and even open and breaking itself during preparation of the cross-sectioning procedure. The surface morphology was rather rough.

Calo-grinding supported the impressions gained by the SEM analyses qualitatively. Figure 8a clearly outlines the ramping socket below the TiAlVN film. On one hand, the **Type 1** film itself appeared entirely structureless now. On the other hand, the **Type 2** film was characterized by a dominating distinct layered structure, as expected from Figure 7b.

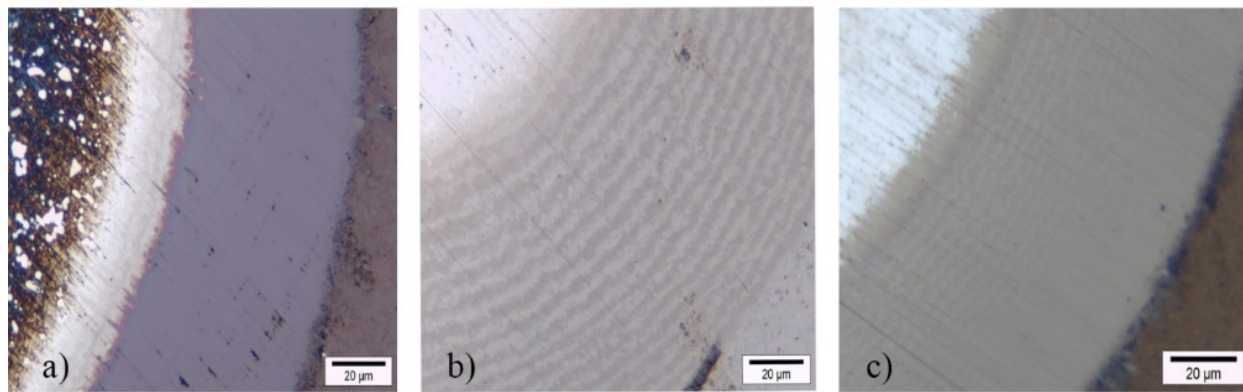


**Figure 8.** Calo grinding: (a) **Type 1**: no chromium; (b) **Type 2**: high chromium content; (c) **Type 3**: low chromium content.

The darker layers obviously represent TiAlVN, whereas CrN-rich layers seemed to turn out much brighter. The thickness of a double layer could be estimated at approximately 0.07 µm. The color of the outer cross sections correlated with the silvery surface color of the test sample perfectly. The thickness of the double layer seemed to shrink during film growth, indicating slight target poisoning with increasing film growth. Only vague layering was indicated by sample **Type 3**. Close to the interface, some weak layers could be observed (Figure 8c). In comparison to Figure 8b, chromium seemed to be distributed rather evenly over the entire cross section, but led to a brighter visual color tone as compared to Figure 8a. However, at the film surface, we observed a narrow violet seam generated by the 5 min deposition of TiAlVN.

The crystal structure was explored by XRD (Seifert PAD II, Detector Meteor 1D, Ahrensburg, Germany). Figure 9 shows the diffraction diagrams of the three film types investigated. The XRD reflexes are highlighted by green dots. The spectra are superimposed with signals stemming from the substrate material (mechanically polished). In general, all three types of films condensed in the fcc crystal structure.

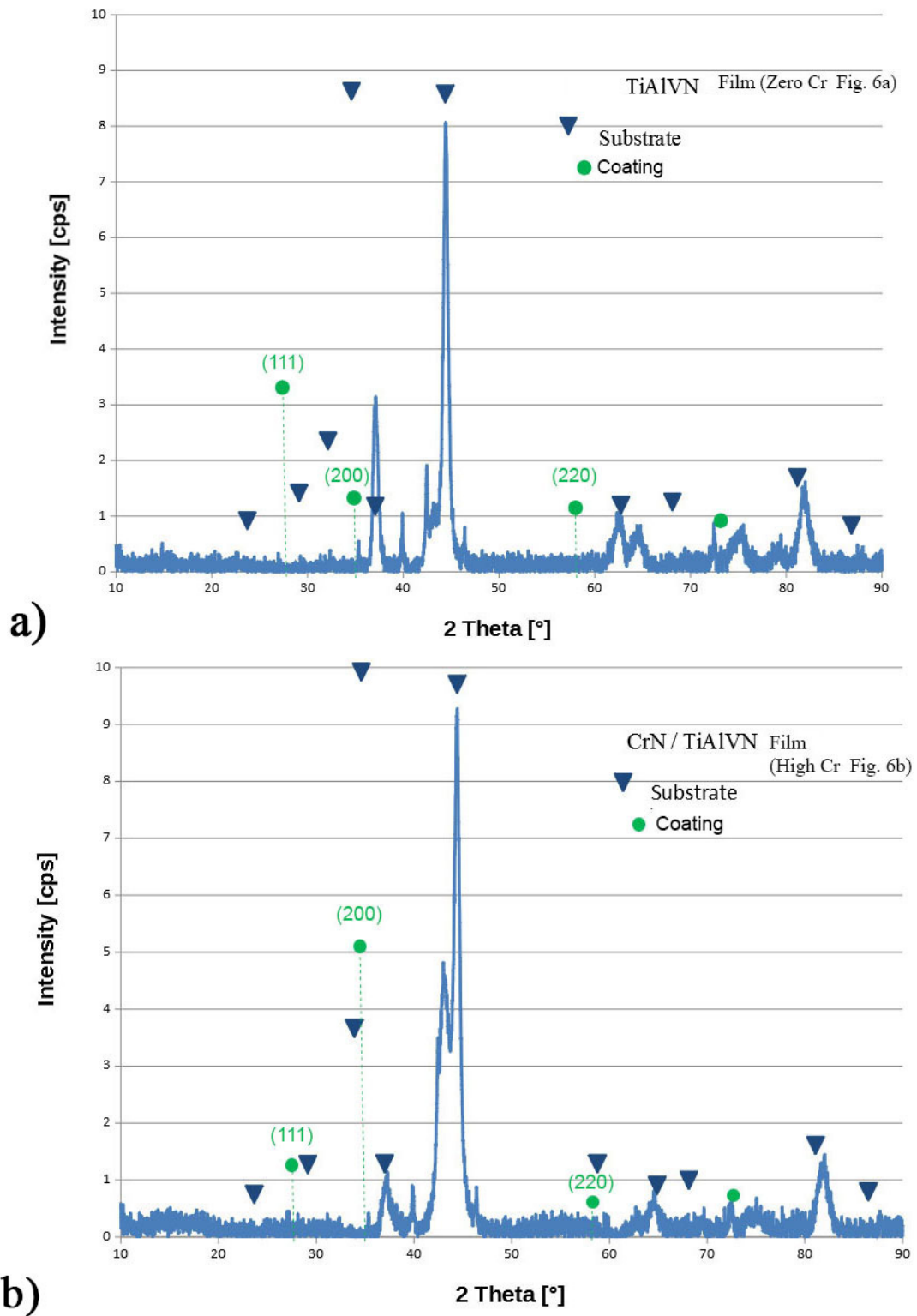
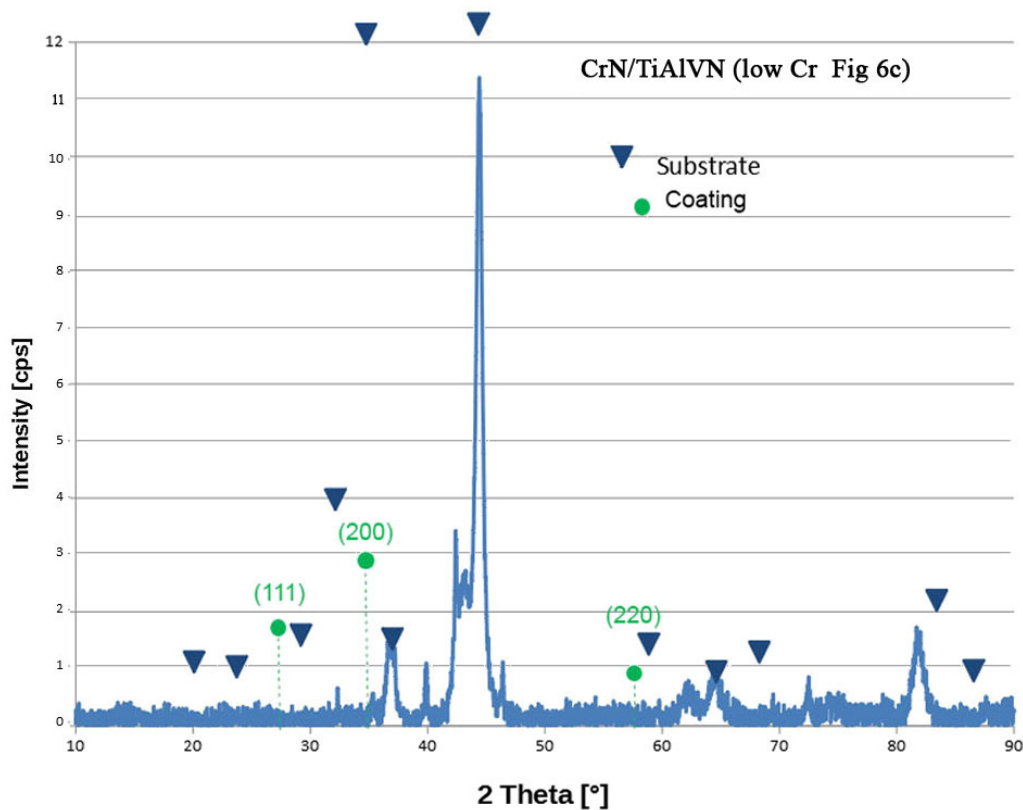


Figure 9. Cont.



c)

**Figure 9.** Crystal structure XRD analyses: (a) **Type 1:** preferred (111); (b) **Type 2:** preferred (200); (c) **Type 3:** randomly orientated.

As expected, the **Type 1** film was characterized by a dominating (111) orientation, with weaker signals indicating (200), (220), and (311) orientations [3]. The intensity ratio (111)/(200) reached 3.0. In contrast, **Type 2** showed an even stronger dominating (200) orientation, with an intensity ratio (200)/(111) of 4.4. This result may be explained by the fact that stoichiometrically grown HIPIMS CrN crystallizes in (200) orientation, principally /18/. The strong (200) orientation of CrN rigorously suppressed the typical (111) orientation of TiAlVN, as highlighted in Figure 9a. In contrast, Figure 9c reveals rather weak reflexes caused by the lower CrN content and the open film morphology. The intensity ratio (200)/(111) dropped down to 1.9. This result could be correlated with the weak layering effect (Figure 7c) located close to the interface regime only.

Regarding the **Type 3** coating, the experiment with reduced HIPIMS power is on the idea of achieving finer-layer structures to meet the expectations of higher hardness values raised by the “superlattice” concept [12]. However, this attempt failed. The reason for this failure might have been a heavy mismatch of the deposition parameters. The HIPIMS process is rather sensitive to target poisoning. However, the reactive gas flow was reduced according to the lower power dissipation as compared with the **Type 2** film, and the nitrogen flow must have been sufficiently high to poison the lower-powered chromium targets, and target poisoning led to a reduced chromium sputter rate. The reactive gas flow was controlled by constant total pressure. Consequently, the resulting increase in nitrogen partial pressure must have been consumed by the Ti-rich targets, therefore causing a poisoning effect as well. As a consequence, the deposition rate of the **Type 3** coating was dramatically lower, namely 0.23 nm/s as compared to **type 2** coating of 0.51 nm/s, not only due to the reduced HIPIMS power, but also due to the side effects of poisoned titanium-rich targets. This should be seen as a warning concerning the delicate interaction of simultaneous UBM and HIPIMS deposition processes. The target poisoning described

for the **Type 3** coating could serve as explanation for the layer-shrinking effect in context with the **Type 2** coating, as speculated in Figure 8b.

### 3.2. Typical Tribological Properties

Results for the tribological properties are summarized in Table 1 below. The following test procedures were executed: the film thickness was evaluated by interpretation of the SEM images; hardness values were evaluated using a conventional Fischer Pico Indenter (Helmut Fischer GmbH, Sindelfingen, Germany); Rockwell indentation results were obtained by indenting a 200  $\mu\text{m}$  diamond ball under a load of 150 kg; the observed indentation patterns were evaluated by SEM and correlated with the well-known “1” to “6” scale; and critical load results were evaluated by increasing the load on a Rockwell C indenter linearly from 10 to 50 N, followed by microscopic interpretation.

**Table 1.** Tribological properties.

Property	Type 1	Type 2	Type 3
Thickness ( $\mu\text{m}$ )	2.2	1.6	1.6
Hardness HV	2000	2800	2500
Rockwell (class “1” to “6”)	“1”	“1”	“1”
Critical load (N)	49	44	47
Friction coefficient	0.73	0.7	0.93
Ball wear ( $\mu\text{m}$ )	786	720	1452
Sliding wear rate ( $10^{-15} \text{ m}^3/\text{Nm}$ )	9.08	12.91	11.43

Friction coefficients were evaluated by ball-on-disc tests against an HRC 6 ball. Finally, the wear rates were determined by employing the FH calomax NT test using an Al-oxide paste.

The results obtained revealed hardness values between HV 2000 (Type 1) and HV 2800 (Type 2), the multilayer (TiAlV/Cr)N coating. Considering the coarse microstructure of the Type 3 coating the hardness still reached HV 2500. HV 2000 seemed rather low compared to the originally reported values for TiAlN deposited in a “twin cathode” arrangement (HV 2500) [3]. All three coatings provided a top-class “1” marking. The critical load values confirmed the excellent Rockwell marks, with values ranging from 44 to 49 N. Friction coefficients of the Type 1 and Type 2 coatings were similar at 0.73 and 0.70, respectively. The slightly lower value of the multilayer coating also was consistent with the somewhat smoother surface structure (compare Figure 7a,b). The friction coefficient of the Type 3 film showed a clearly higher value of 0.93, obviously due to the rather coarse surface microstructure, as documented in Figure 7c, independent of the thin low-friction topcoat of TiAlVN. We obtained analogue results concerning the ball wear. The low-friction Type 1 and Type 2 samples wore off the steel ball to a lesser degree than the coarser-structured Type 3 coating. Therefore, the chromium-containing coatings wore off somewhat faster, although they exhibited higher hardness values.

In summary, the results show by the Type 2 film were quite satisfying. They compared well with values published elsewhere. However, the most important industrial relevance consisted of the enhanced deposition rate of 0.51 nm/s by utilizing the appropriate simultaneous operation of HIPIMS and UBM cathodes during the film deposition.

Consequently, the wear behavior of the Type 2 coating, which was extremely interesting industrywise, was compared with practiced state-of-the-art coatings deposited by cathodic arc.

### 3.3. Examples of First Cutting Tests

The actual wear of broaches can be analysed realistically in industrial lifelong tests only. It is rather intriguing to determine the wear quantitatively on the complicated and very expensive tools directly. Therefore, a “shaping” test was introduced to evaluate the wear behavior of hard coatings common in the field on specially designed test samples

(model tooth). Figure 10 shows a schematic of the test method using experimental shaping equipment.

### Test conditions:

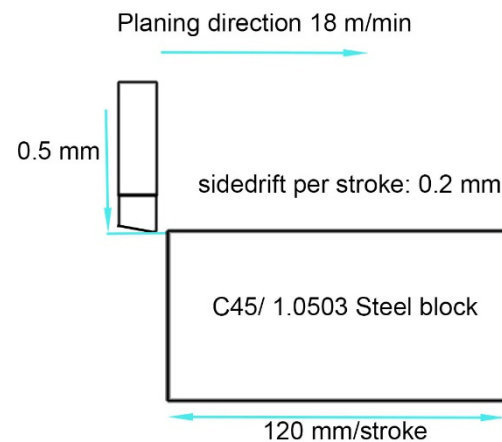


**Figure 10.** “Shaping” test equipment.

The wear/cutting tests were performed on a C45 steel block. The model tooth in the test was moved at a shaping speed of 18 m/min, digging a 0.5 mm wide, 120 mm long deep groove into the steel. The test piece was multifold passed with a side/drift of 0.2 mm per stroke across the test material until a total cutting length of 210 m was achieved. Two 2  $\mu$ m thick coatings were compared. A state-of-the-art cathodic arc, in-house-coated TiN model tooth served as a comparison, as stated above. This model tooth was coated in an industrial PVD coater made by the Arthur Klink Company (Pforzheim, Germany) dedicated to coating broaches. As indicated above, TiN was compared with the new Type 2 (TiAlV/Cr)N coating. Figure 11a,b outlines the test results.

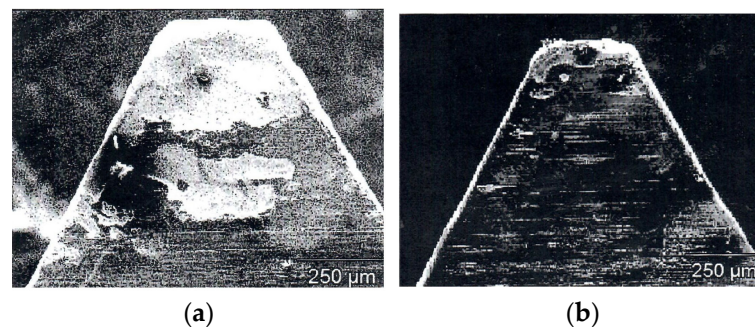


**Figure 11.** Comparison of wear performance: (a) TiN-coated sample; (b) (TiAlV/Cr)N-coated sample.

The test TiN sample showed substantial wear on the tip point of the model tooth (very bright seam) as well as serious film flaking on the area close to the top. Serious wear was also found on the side edges of the test sample. In contrast, we observed much reduced wear on the tip point of the (TiAlV/Cr)N-coated test piece. In addition, the progress in wear on the side edges was also comparably negligible as compared to the TiN-coated sample. If we neglected the tremendous flaking on the TiN-coated sample, an improvement in the overall shaping performance by an estimated factor of 2 to 3 may certainly be expected.

To explore the cutting performance of a relevant broach, a special tool has been designed by the Arthur Klink Company. This tool reached a length of 3 m and a diameter of 60 mm. The tool has been coated either with 3  $\mu$ m thick standard Arthur Klink Company produced cathodic arc TiN and the investigated (TiAlV/Cr)N. In addition the (TiAlV/Cr)N

coating was topped with a 0.5  $\mu\text{m}$  thick low-friction **Type 1** film (Figure 12). The dark violet topcoat allowed better judgment of the progressing wear on the metallic cutting edge due to the improved visual contrast-free metal and a “more or less decorative help” topcoat as compared with the silvery color tone of the (TiAlV/Cr) coating.



**Figure 12.** Model broach coated with **Type 1** and **Type 2** films.

Finally, the cutting performance of the above-mentioned 1.3 m long model broach was investigated. Again, the two types of coatings, TiN and (TiAlV/Cr)N, were compared.

The success of a tool coating depends on various aspects. As could be derived from the drilling tests, a TiN coating allowed a multifold improvement in lifetime as compared to uncoated HSS tools. The TiAlN-based coating was developed in particular for dry, high-speed machining. The actual lifetime of the expensive broaches was evaluated at end users' sites routinely. Exposing both test model broaches to identical high-speed cutting conditions defined by the end user, an improvement in tool lifetime of 150% was reported in the context of the new (TiAlV/Cr)N coating in comparison to TiN. The wear was evaluated directly on the cutting edge, indicated by bright metallic areas freed from the dark coating.

Finally, a short insight into economic considerations will be given (Table 2). Although the coating times of various-sized tools depends strongly on their diameter, the loading capacity of the coating equipment, as well as on the actual status of system cleanness (residual gas pressure), the following estimates of the coating times of the three types of coating described above, relevant to 60 mm diameter broaches, will be given, including pump down, in vacuo pretreatment, and real coating time, but without cool down time:

**Table 2.** Productivity of the investigated coatings.

Type	Actual Coating Time	Total Process Duration
Type 1	105 min	265–325 min
Type 2	52 min	110–270 min
Type 3	200 min	350–450 min

#### 4. Conclusions

The results presented here show that magnetron sputtering technology can be applied successfully to deposit well-adherent, dense, and wear-resistant hard coatings onto test substrates and broaches, although our test samples were passing and rotating at varying near and far distances from the cathodes during film deposition. The **Type 2** coating turned out to be the clear favourite in the project presented here. Excellent results were achieved, particularly with respect to hardness, adhesion, and wear performances. Furthermore, the simultaneous UBM/HIPIMS provided enhanced deposition rates when the interaction of UBM and HIPIMS concerning DC and pulse power levels, as well as reactive gas flows, were optimized accordingly.

Finally, the new segmented UBM process approach provides advantages with respect to industrial throughput when following the described equipment design.

**Author Contributions:** Conceptualization, methodology, validation, W.-D.M. and R.K.; formal analyses and investigation, R.K. and D.A.; writing—original draft preparation, W.-D.M.; writing—review and editing, W.-D.M.; process control and production supervision, R.K. and D.A.; film analyses, D.A. and M.M. All authors have read and agreed to the published version of the manuscript.

**Funding:** This research received no external funding.

**Institutional Review Board Statement:** Not applicable.

**Informed Consent Statement:** Not applicable.

**Data Availability Statement:** Not applicable.

**Acknowledgments:** Particular gratitude is directed to Werner Klink, CEO of Arthur Klink Company, Pforzheim, who supported confidence planning and managing the creation of the described PVD machine. Furthermore, we acknowledge the continuous encouragement by Joe E. Greene and Ivan G. Petrov, University of Illinois, by supplying scientific support. Finally, we would like to acknowledge the support of scientists Leiste and Stüber of the Karlsruhe Institute of Technology (KIT), Germany, who helped with the excellent XRD and EDX film analyses in this project. The authors are also grateful for the tribological results and SEM analyses, which were contributed by experts Lisa Döring and Thorsten Zufass of SYSTEC Comp., Karlstadt am Main, Germany.

**Conflicts of Interest:** The authors declare no conflict of interest.

## References

1. Broaching (Metalworking). Available online: [https://en.wikipedia.org/wiki/Broaching\\_\(metalworking\)](https://en.wikipedia.org/wiki/Broaching_(metalworking)) (accessed on 10 September 2017).
2. Oerlikon Balzers GmbH Internet. Plasma-Assisted Coating Processes (Balzers, Liechtenstein). Available online: <https://www.oerlikon.com/balzers/global/en/> (accessed on 21 November 2021).
3. Münz, W.-D. Titanium aluminium nitride: A new alternative to TiN coatings. *J. Vac. Sci. Technol. A* **1986**, *4*, 2117–2225. [CrossRef]
4. Münz, W.-D. Unbalanced magnetrons: Their impact to modern PVD PVD hard coating equipment. *Ann. Technol. Conf. Proc. SVC* **1992**, *1-878068-11-3*, 243.
5. Mayrhofer, P.H.; Hovsepian, P.E.; Mitterer, C.; Münz, W.-D. Calorimetric evidence for frictional self-adaption on TiAlN/VN superlattice coatings. *Surf. Coat. Technol.* **2004**, *177–178*, 341–347. [CrossRef]
6. PalDaley, S.; Deevi, S.C. Single layer and multilayer coatings of (TiAl)N: A review. *Mater. Sci. Eng. A* **2003**, *324*, 58. [CrossRef]
7. Brown, G.; Feinberg, B.; Galvin, J.E. Multiply stripped ion generation in the metal vapor vacuum arc. *J. Appl. Phys.* **1988**, *63*, 4889–4898. [CrossRef]
8. Schönjahn, C.; Donohue, L.A.; Lewis, D.B.; Münz, W.-D.; Twesten, R.D.; Petrov, I. Enhanced adhesion through local epitaxy of transition-metal nitride coating ferritic steel promoted by metal ion etching in combined cathodic arc/unbalanced magnetron deposition systems. *J. Vac. Sci. Technol. A* **2000**, *18*, 1718–1723. [CrossRef]
9. Münz, W.-D.; Hauzer, F.J.M.; Schulze, G.; Buil, B. A new concept of physical vapor deposition combining the method of arc evaporation and unbalanced magnetron sputtering. *Surf. Coat. Technol.* **1991**, *49*, 161–167. [CrossRef]
10. Hauzer, F.J.M.; Münz, W.-D.; Schulze, B.J.A.M.B.D.; Tietema, R. Arc Magnetron and the Method of Coating. U.S. Patent US00516095, 3 November 1992.
11. Münz, W.-D.; Zufass, T. Industrial scale deposition of well adherent superhard and low friction C-DLC coatings grown by HIPIMS and anode assisted unbalanced magnetron sputtering. *Surf. Coat. Technol.* **2020**, *387*, 125485. [CrossRef]
12. Münz, W.-D. Large Scale Manufacturing of Nanoscale Multilayered Hard Coatings Deposited by Cathodic Arc/Unbalanced Magnetron Sputtering. *MRS Bull.* **2003**, *28*, 173–179. [CrossRef]
13. Münz, W.-D.; Smith, I.J.; Lewis, D.B.; Creasey, S. Dorplet formation on steel substrates during cathodic arc metal ion etching. *Vacuum* **1997**, *48*, 473–481. [CrossRef]
14. Kouznetsov, V.; Macak, M.; Schneider, J.M.; Helmersson, U.; Petrov, I. A novel pulsed magnetron sputter technique utilizing very high target power densities. *Surf. Coat. Technol.* **1999**, *122*, 290–293. [CrossRef]
15. Ehasarian, A.; New, R.; Münz, W.-D.; Hultman, L.; Helmersson, L.; Kouznetsov, V. Influence of high power densities on the composition of pulsed magnetron plasmas. *Vacuum* **2001**, *65*, 147–154. [CrossRef]
16. EU Growth Project (CRAFT). “NEW CHROME” Cont. Nr. G5ST-CT-2002-530355, Engineering HIPIMS. Coord.: W.-D. Münz.
17. Münz, W.-D. *HIPIMS: The New PVD Technology, Vacuum's Best VIP*; Wiley-VHC Verlag GmbH & Co. KgaH: Weilheim, Germany, 2008.
18. Ehasarian, A.P.; Münz, W.-D.; Hultman, L.; Helmersson, U.; Petrov, I.G. High power pulsed magnetron sputtered CrN films. *Surf. Coat. Technol.* **2003**, *163–164*, 267–272. [CrossRef]
19. Münz, W.-D.; Ehasarian, A.; Hovsepian, P.E. PVD Coating Process Magnetron Cathodic Sputtering. European Patent EP 1 260 603, 21 May 2002.

20. Münz, W.-D.; Schenkel, M.; Kunkel, S.; Paulitsch, J.; Bewilogua, K. Industrial Applications of HIPIMS. *J. Phys. Conf. Ser.* **2008**, *100*, 082100. [[CrossRef](#)]
21. Paulitsch, J.; Mayrhofer, P.H.; Münz, W.-D.; Schenkel, M. Structure and mechanical properties of CrN/TiN multilayer coatings prepared by combined HIPIMS/UBM deposition technique. *Thin Solid Films* **2008**, *517*, 1239–1244. [[CrossRef](#)]
22. Paulitsch, J.; Schenkel, M.; Zufass, T.; Mayrhofer, P.H.; Münz, W.-D. Structure and properties of high power impulse magnetron and DC magnetron sputtering CrN and TiN films deposited in an industrial scale unit. *Thin Solid Films* **2010**, *518*, 5558–5564. [[CrossRef](#)]
23. OES Was Supplied by: PLASUS—Plasma Monitor and Process Control Systems. Available online: <https://www.plasus.de/en/> (accessed on 10 September 2017).
24. Pflüger, E.; Schroer, A.; Voumard, P.; Donohue, L.A.; Münz, W.-D. Influence of incorporation of Cr and Y on wear performance of TiAlN coatings at elevated temperatures. *Surf. Coat. Technol.* **1999**, *115*, 17–23. [[CrossRef](#)]
25. Hovsepian, P.E.; Lewis, D.B.; Luo, Q.; Münz, W.-D.; Mayrhofer, P.H.; Mitterer, C.; Zhou, Z.; Rainforth, W.M. TiAlN based nanoscale multilayer coatings designed to adapt tribological properties at elevated temperatures. *Thin Solid Films* **2005**, *485*, 160–168. [[CrossRef](#)]
26. Zlatanovic, M.; Münz, W.-D. Wear resistance of plasma-nitrided and sputter ion-plated hobs. *Surf. Coat. Technol.* **1990**, *41*, 17–30. [[CrossRef](#)]